Secondary Binding Site of the Potato Carboxypeptidase Inhibitor. Contribution to Its Structure, Folding, and Biological Properties†

Joan L. Arolas, Julia Lorenzo, Ana Rovira, Josep Vendrell, Francesc X. Aviles,* and Salvador Ventura

Institut de Biotecnologia i de Biomedicina and Departament de Bioquímica i Biologia Molecular, Universitat Autònoma de Barcelona, 08193 Bellaterra, Spain

Received February 27, 2004; Revised Manuscript Received April 15, 2004

ABSTRACT: The contribution of each residue of the potato carboxypeptidase inhibitor (PCI) secondary binding site to the overall properties of this protein has been examined using alanine-scanning mutagenesis. Structural and enzymatic studies, performed on a series of PCI mutants, demonstrate that the proper positioning of the primary site for efficient binding and inhibition of carboxypeptidase A is significantly dependent on such a secondary contact region. The aromatic residues in this region play a key role in the stabilization of the PCI−enzyme complex, whereas polar residues contribute little to this task. A comparative study of the oxidative folding of these PCI mutants has been carried out using the disulfide quenching approach. The data, together with the structural characterization of some of these mutants, clearly indicate that noncovalent forces drive the refolding of this small disulfide-rich protein at the reshuffling stage, the rate-limiting step of the process. Moreover, it reveals that by introducing new noncovalent intramolecular contacts in PCI, we may create more stable variants, which also show improved folding efficiency. Taken together, the collected results clarify the folding determinants of the primary and secondary binding sites of PCI and their contribution to the inhibition of the carboxypeptidase, providing clues about PCI evolution and knowledge for its biotechnological redesign.

In the past several years, much effort has been devoted to understanding the interactions that drive the formation of protein−protein complexes (*1*−*3*). The associations between proteases and their specific inhibitors are very adequate as models for such studies given the large number of different species, structures, and stabilities that are encompassed (*4*). The detailed characterization of the energetic and structural basis that lay behind protease−inhibitor interactions is also of great biotechnological relevance because of their involvement in fundamental biological processes, such as insect attack−vegetal defense strategies, parasite invasion, blood coagulation and fibrinolysis, inflammation, local anaphylaxis, fertilization, hormone and neuropeptide processing, carcinogenesis, and invasiveness, among others (*5*−*8*).

The carboxypeptidase inhibitor (PCI)[1] is a small, 39-amino acid, globular protein naturally occurring in potatoes that can competitively inhibit several carboxypeptidases, forming complexes with an inhibition constant (K_i) in the nanomolar range (*5*, *9*). Its structure has been studied in detail in solution by NMR (*10*, *11*) and by X-ray crystallography in complex with bovine carboxypeptidase A (CPA) (*12*). This small protein is folded into a 27-residue globular core that lacks regular secondary structures, except for a short five-residue helix and a very small β-sheet, and is stabilized by three disulfide bridges. PCI shares a peculiar disulfide-stabilized loop scaffold, known as the cystine knot or T-knot, with other plant protease inhibitors and with animal peptidic growth factors, such as the epidermal growth factor (EGF) (*13*). From its hydrophobic central core protrudes a five-residue C-tail (residues 35−39), which is inserted into the active site of the carboxypeptidase and shapes the primary binding site with the enzyme. A short stretch of core residues located around Trp28 (residues 15, 22, 23, and 28−30) constitutes the secondary binding site (*12*). The contribution of the primary binding site of PCI both to the formation of its complex with CPA and to its thermodynamic stability has been previously evaluated in detail using a site-directed mutagenesis approach (*14*, *15*). These studies suggested that, in addition to the C-terminal tail of PCI, the secondary binding site also plays an important role in PCI function.

The folding process of small disulfide-rich proteins is strongly driven and constrained by the proper disulfide bond formation. The folding reaction of these proteins can be studied using the disulfide acid-trapping approach, in which the folding intermediates that form during their oxidative refolding are trapped at low pH, purified by reversed-phase high-performance liquid chromatography (RP-HPLC), and analyzed (*16*, *17*). On the other hand, their unfolding pathways and conformational stabilities can be assayed by disulfide scrambling, based on the observation that the

† This work has been supported by Grant BIO2001-2046 (Ministerio de Ciencia y Tecnología, MCYT, Spain) and by the Centre de Referència en Biotecnologia (Generalitat de Catalunya, Spain). S.V. is supported by a "Ramón y Cajal" project awarded by the MCYT and cofinanced by the Universitat Autònoma de Barcelona. J.L.A. is a recipient of a fellowship from the Universitat Autònoma de Barcelona.

* To whom correspondence should be addressed. E-mail: fxaviles@einstein.uab.es. Telephone: 34-93-581-1315. Fax: 34-93-581-2011.

[1] Abbreviations: CD, circular dichroism; CPA, carboxypeptidase A; Cys, cysteine; Cys-Cys, cystine; D/H, deuterium to proton; EGF, epidermal growth factor; GdnHCl, guanidine hydrochloride; K_i, inhibition constant; MALDI-TOF MS, matrix-assisted laser desorption/ionization time-of-flight mass spectrometry; PCI, potato carboxypeptidase inhibitor; RP-HPLC, reversed-phase high-performance liquid chromatography; TAFI, thrombin-activatable fibrinolysis inhibitor; TAP, tick anticoagulant peptide; TFA, trifluoroacetic acid; WT, wild-type.

10.1021/bi049596j CCC: $27.50
Published on Web 05/26/2004

presence of trace amounts of a thiol initiator during unfolding by denaturants generates a mixture of native and disulfide-scrambled species (*18*, *19*).

In PCI, as in hirudin, EGF, or tick anticoagulant peptide (TAP), the folding of the fully reduced and denatured protein to the native form proceeds through an initial stage of nonspecific disulfide formation (packing), followed by a rate-limiting step of disulfide reshuffling of partially packed intermediates to acquire the native structure (consolidation) (*20*−*27*). These small disulfide-containing proteins seem also to share a common unfolding pathway that encompasses a gradual expansion and relaxation of the polypeptide conformation toward a more linear structure (*18*, *19*, *28*). In addition, PCI is an example of protein sequences that are unable to fold quantitatively into single native structures, since scrambled isomers exist in equilibrium with the native fold under physiological conditions (*28*).

In the work presented here, we have used alanine-scanning mutagenesis (*29*, *30*) to gain insights into the role of secondary binding site residues in the folding, structure, and function of PCI. The analysis of the inhibitory, conformational, thermodynamic, and folding characteristics of the different protein mutants has allowed us to dissect the individual contribution of each residue of the secondary binding site in PCI properties. Potential biotechnological applications of these results are discussed.

EXPERIMENTAL PROCEDURES

Materials. All chemicals used in DNA manipulation procedures and the oligonucleotides for site-directed mutagenesis were obtained from Roche Applied Science. Cysteine (Cys), cystine (Cys-Cys), urea, guanidine hydrochloride (GdnHCl), 2-mercaptoethanol, and dithiothreitol, with purities of >99%, were purchased from Sigma. The chromogenic substrate *N*-(4-methoxyphenylazoformyl)-L-phenylalanine was obtained from Bachem. Bovine CPA was from Sigma.

Molecular Cloning and Site-Directed Mutagenesis. The synthetic gene for PCI (*31*) was cloned into the pBAT4 plasmid, fused in frame to the OmpA signal sequence.[2] Site-directed mutagenesis was performed on this construction using the QuickChange site-directed mutagenesis kit from Stratagene according to the procedure recommended by the manufacturer. F23A and N29A mutants were used as templates in the PCR to generate PCI forms F23A/W28A and N29A/S30A, respectively. All constructs were verified by DNA sequencing.

Protein Expression and Purification. Recombinant PCI forms were obtained by heterologous expression in *Escherichia coli* strain BL21(DE3). Proteins were purified from the culture medium using a Sep Pak C_{18} cartridge (Waters), followed by anion exchange chromatography on a TSK-DEAE 5PW column (Tosohaas) and by gel filtration chromatography on a Superdex Peptide column (Amersham Biosciences). Molecular masses were confirmed by matrix-assisted laser desorption/ionization time-of-flight mass spectrometry (MALDI-TOF MS). The concentration of the purified solutions of recombinant PCIs was determined from the A_{280} of the final solution (PCI extinction coefficient $E_{0.1\%}$ = 3.0). For mutants lacking a Trp residue, the extinction coefficient ($E_{0.1\%}$) was estimated to be 1.7 from the sequence.

Oxidative Refolding. The native protein (0.2 mg/mL) was dissolved in Tris-HCl buffer (0.5 M, pH 8.4) containing 5 M GdnHCl and 30 mM dithiothreitol and kept at 23 °C for 2 h. The reduced and denatured sample was then passed through a PD-10 gel filtration column (Amersham Biosciences) previously equilibrated with Tris-HCl buffer (0.1 M, pH 8.4). The protein was eluted in 1.2 mL and split in three parts that were immediately diluted in the same Tris-HCl buffer to a final protein concentration of 60 mg/mL, in the absence (control −) and presence of Cys (1 mM) or Cys and Cys-Cys (4 and 2 mM, respectively). In some cases, refolding experiments were carried out at a concentration of 0.5 mg/mL in the Tris-HCl buffer, both in the absence (control −) and in the presence (control +) of 0.25 mM 2-mercaptoethanol. Folding intermediates were trapped in a time course manner at selected times by mixing aliquots from the different solutions with an equal volume of 2% trifluoroacetic acid (TFA) in water and analyzed by RP-HPLC on a Protein C_4 column (Vydac, 4.6 mm × 150 mm). Using water containing 0.1% TFA as solvent A and acetonitrile containing 0.1% TFA as solvent B, a linear gradient from 20 to 40% B over the course of 30 min was applied, at a flow rate of 0.75 mL/min.

Denaturation and Unfolding in the Presence of a Denaturant. The native protein (0.5 mg/mL) was dissolved in Tris-HCl buffer (0.1 M, pH 8.4) containing 0.25 mM 2-mercaptoethanol and selected concentrations of denaturants (urea and GdnHCl). The reaction was allowed to reach equilibrium and was typically performed at 23 °C for 20 h. The reactions were then quenched with 2% TFA and analyzed by HPLC using the same conditions described in Oxidative Refolding. To follow the time course of unfolding, the native protein (0.5 mg/mL) was dissolved in the same buffer containing 6, 7, or 8 M GdnHCl. At given incubation times, aliquots were removed, the reactions were quenched with 2% TFA, and the mixtures were analyzed by HPLC.

Reductive Unfolding. The native protein (0.5 mg/mL) was dissolved in Tris-HCl buffer (0.1 M, pH 8.4) containing 5 mM dithiothreitol. Reduction was carried out at 23 °C. To monitor the kinetics of unfolding, aliquots of the sample were removed at various time intervals, the reactions were quenched with 2% TFA, and the mixtures were analyzed by HPLC as described in detail in Oxidative Refolding.

Circular Dichroism and NMR Spectroscopy. Samples for circular dichroism (CD) spectroscopy were prepared by dissolving the protein to a final concentration of 0.2 mg/mL in 0.1% aqueous TFA (pH 2.0) or sodium phosphate buffer (20 mM, pH 7.0). CD spectra were collected on a Jasco J-715 spectrometer at 25 °C using a cell with a path length of 2 mm. Protein samples for NMR experiments were prepared by dissolving the protein in H_2O and D_2O (9:1 ratio by volume) at a concentration of ∼2 mM at pH 4.0. NMR spectra were acquired on a Bruker AMX 500 MHz spectrometer at 35 °C.

Deuterium to Proton Exchange Followed by MALDI-TOF MS. The native protein (0.2 mg/mL) was dissolved in deuterated Tris-DCl buffer (0.5 M, pD 8.4) containing 5 M GdnHCl and 30 mM dithiothreitol. The sample was acidified to pH 3.0 and passed through a PD-10 column, equilibrated with glycine buffer (20 mM, pH 3.0). The reduced and

[2] S. Bronsoms et al., manuscript in preparation.

denatured protein was collected and lyophilized. The sample was then refolded in the deuterated Tris-DCl buffer containing Cys and Cys-Cys (4 and 2 mM, respectively). The native deuterated protein was diluted 1:9 with ammonium citrate (50 mM, pH 5.0) to start the hydrogen exchange. Aliquots were taken at different times and analyzed by MALDI-TOF MS on a Bruker Ultraflex spectrometer until an exchange plateau was reached. Samples were prepared by mixing equal volumes of the protein solution and matrix solution (sinapic acid in aqueous 30% acetonitrile with 0.1% TFA). Six samples were analyzed twice at each exchange time. The average of the mass values corresponding to the centroid of the peaks was calculated for each exchange time and compared to an external unlabeled control, whose mass was determined by duplicate measurements.

CPA Inhibitory Assays. Inhibition constants of the different PCI forms were calculated ($K_i = K_{off}/K_{on}$) by pre-steady-state analysis (*32*). Kinetic association (K_{on}) and dissociation (K_{off}) constants were determined by a continuous photometric assay with the chromogenic substrate *N*-(4-methoxyphenylazoformyl)-L-phenylalanine. The assay was performed in Tris-HCl buffer (50 mM, pH 7.5) containing 0.1 M NaCl, with a substrate concentration of 100 mM and a bovine CPA concentration of 2 nM. Several independent K_i determinations were made for each PCI form and corrected for substrate competition. The dissociation free energy of the PCI−CPA complexes was calculated according to the formula $\Delta G_d^\circ = -RT \ln K_i$.

RESULTS

Role of the PCI Secondary Binding Site in CPA Inhibition. In the PCI−CPA complex, the C-terminal amino acid tail of PCI docks into the active site of the enzyme, leading to a stopper-like inhibition mechanism (*5*, *12*). The carboxy-terminal residue of PCI (Gly39) is cleaved off by CPA during the first stages of the binding, and remains bound in the S1′ subsite of CPA. The carboxylate group of the previous residue (Val38) coordinates with the Zn^{2+} of the active site. The rest of the polypeptide chain of PCI remains away from the CPA surface until residues 27−30. These residues pass along the CPA molecule forming a secondary contact region which also includes the side chains of His15, Trp22, and Phe23 (*12*), and is shown in Figure 1. To analyze in a systematic and unbiased way the role and energetic contributions of these residues in the complex, every side chain in this interface was substituted with that of Ala. Moreover, F23A/W28A and N29A/S30A double mutants were produced to asses the additive or cooperative nature of side chain contributions. All mutant proteins were expressed in *E. coli* as secreted soluble proteins and purified to homogeneity, and their identities were confirmed by MS. The purity was greater than 98% in all cases. The RP-HPLC chromatographic retention displayed by the mutants correlated well with the introduced changes in protein polarity due to amino replacements.

The characterization of the interaction of wild-type (WT) PCI and PCI mutants with CPA in terms of their K_i and the free energy of dissociation of the complexes (ΔG_d°) are shown in Table 1. Such results allow us to classify residues of the secondary binding site into two groups according to their binding to CPA and side chain characteristics.

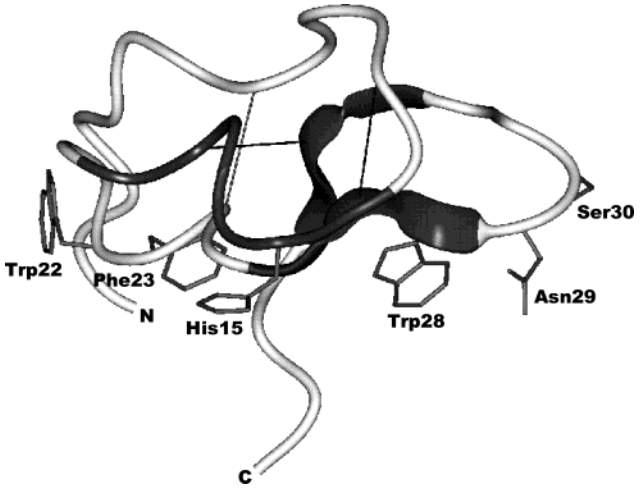

FIGURE 1: Schematic view of the native three-dimensional structure of PCI. The secondary binding site residues are depicted in the structure. N and C denote the locations of N- and C-terminal regions, respectively, of PCI. The Protein Data Bank entry for the structure of PCI is 1H20.

Table 1: Association (K_{on}), Dissociation (K_{off}), and Inhibition (K_i) Kinetic Constants of Wild-Type and Mutant PCIs for CPA and Gibbs Free Energies of Dissociation (ΔG_d°) of the Respective PCI−CPA Complexes

PCI form	K_{on} (M^{-1} s^{-1})	K_{off} (s^{-1})	K_i (nM)	ΔG_d° of the complex (kcal/mol)
WT	2.1×10^6	3.4×10^{-3}	1.6 ± 0.2	12.0
H15A	2.1×10^6	4.8×10^{-3}	2.3 ± 0.3	11.8
W22A	5.2×10^5	4.1×10^{-3}	7.9 ± 0.7	11.1
F23A	1.3×10^5	2.4×10^{-3}	18.5 ± 1.9	10.6
W28A	2.5×10^5	3.3×10^{-3}	13.2 ± 1.5	10.8
N29A	2.6×10^6	4.0×10^{-3}	1.5 ± 0.2	12.0
S30A	3.4×10^6	4.6×10^{-3}	1.4 ± 0.2	12.1
F23A/W28A	8.5×10^3	3.7×10^{-3}	440 ± 37	8.7
N29A/S30A	1.8×10^6	3.4×10^{-3}	1.9 ± 0.4	11.9
N29G	1.1×10^6	3.9×10^{-3}	3.5 ± 0.4	11.5

Role of the Secondary Binding Site Polar Residues in CPA Inhibition. In the PCI−CPA complex, residues Asn29 and Ser30 of PCI are hydrogen bonded to the main chain of residues Ile247 and Thr246 of CPA, respectively. The change of either Asn29 or Ser30 to Ala did not significantly affect the K_i value of the binding, with K_{on} and K_{off} values of the mutant proteins being very similar to those of the WT form. Also, the double Ala mutant (N29A/S30A) retains an inhibitory activity identical to that of WT PCI, clearly indicating that the polar side chains of these residues are not involved in the stabilization of the PCI−CPA complex (Table 1). In the PCI−CPA crystal structure, a hydrogen bond is established between the imidazole group of His15 and the CPA Tyr248 side chain ring. This contact, again, does not seem to be relevant for complex formation or stabilization since the His to Ala substitution results in just a very moderate increase in the K_i value (Table 1).

Role of the Secondary Binding Site Aromatic Residues in CPA Inhibition. The aromatic residues of the secondary binding site of PCI (Trp22, Phe23, and Trp28) appear to play an important role in its inhibitory capability. All these aromatic nonpolar side chains are solvent-exposed in the uncomplexed molecule, and their mutation to Ala results in PCI variants with seriously decreased inhibitory activity (Table 1). Thus, mutant W22A exhibited a nearly 5-fold

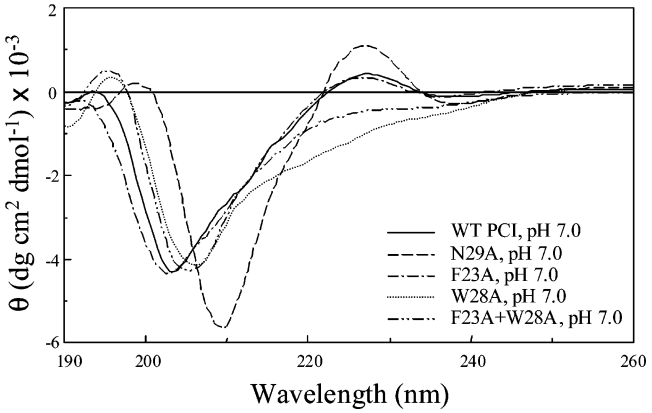

FIGURE 2: Circular dichroism spectra of PCI forms. CD analyses of native and mutant PCI forms were carried out in 0.1% aqueous trifluoroacetic acid (pH 2.0) and in sodium phosphate buffer (20 mM, pH 7.0) with a protein concentration of 0.2 mg/mL. Spectra were very similar for each PCI form under both pH conditions.

increase in the K_i compared to that of WT PCI. As deduced from the crystal structure of the WT complex, this mutant would lose interactions with side chains of CPA residues Phe277 and Arg276. Substitution of Phe23 with Ala caused the largest effect on the inhibitory activity of PCI, with an approximately 12-fold increase in the K_i, indicating that the side chain of Phe23 contributes with 1.4 kcal/mol to the binding energy of the complex. From such a significant contribution, and from the crystal structure, it can be deduced that this mutant would be unable to establish an important interaction with the Phe279 aromatic ring of CPA. In addition, Phe23 of PCI accounts for 21% of the surface area buried in the secondary binding region, and its mutation to Ala diminishes the size of the PCI−CPA contact surface. The third mutant, W28A, exhibited a K_i ~8-fold higher than that of WT PCI, an effect that could be attributed to the loss of the interactions with residues Tyr198, Ser199, and Leu202 of CPA.

Finally, the double substitution F23A/W28A caused a dramatic decrease in inhibitory activity toward CPA, with a K_i that is ~275 times greater than that of WT PCI. From the measured rate constants, it can be seen that such an increase in K_i is mainly due to its slow association with CPA ($K_{on} = 8.5 \times 10^3$). It is worth mentioning that the double mutation causes a 3.3 kcal/mol decrease in the binding energy, which is greater than the 2.6 kcal/mol value expected from a simple additive effect, indicating that a coordinated action of both aromatic side chains takes place in the stabilization of the PCI−CPA complex.

Structural Reasons behind the Role of Phe23 and Trp28 in Complex Stabilization. The conformation of the singly and doubly Ala-substituted mutants was analyzed by CD and NMR spectroscopy in an effort to understand the enthalpic contribution of both Phe23 and Trp28 residues to CPA binding. Although PCI has a small content of secondary structures, far-UV CD spectroscopy was previously reported to be a helpful tool in monitoring the conformational state of PCI variants (*21*). PCI displays a peculiar CD spectrum with a strong minimum of ellipticity at 204 nm and a maximum at 228 nm, the latter being due to residue Tyr37 (Figure 2) (*21*). Interestingly, the scrambled forms of WT PCI, which possess all the residues of the native form but display different conformations, lack this maximum that could thus be attributed to a native-like environment around Tyr37.[3] The CD spectrum of the F23A mutant is very similar to that of the WT protein, while the positive band at 228 nm is absent in both the W28A and F23A/W28A mutants (Figure 2). It suggests that a native-like conformation prevails in the first case and that Tyr37 is not properly oriented in the last two mutants.

We have recently shown by NMR that the conformation of PCI in solution does not differ in general terms from that adopted in the crystal when complexed to CPA (*11*). In the work presented here, homonuclear two-dimensional (2D) NMR studies of selected PCI mutant forms were carried out at pH 4.0 and 35 °C. In accord with CD data, both the fingerprint and NH−NH regions of the F23A mutant are very similar to those in the NMR spectra of the WT form (Figure 3A,B), indicating that no important changes in the globular structure of PCI are introduced by this mutation. Thereby, its increased K_i toward CPA can be mainly assigned to the truncation of the Phe23 side chain, which renders this mutant unable to establish proper interactions with CPA.

In contrast, when compared to WT PCI, the low signal dispersion in the one-dimensional (1D) NMR spectra, the scarce spatial contacts in the fingerprint region and some weaker cross-peaks in the NH−NH region suggest that the mutant W28A has a high degree of flexibility and probably a less compact globular nucleus. In particular, C27−W28, K10−C34, W28−G35, R32−T33, T33−G35, and C34−G35 contacts are lost in this mutant (Figure 3C). Previous molecular dynamics studies have suggested that the contacts of Trp28 with Gly35 could play an important role in the maintenance of the C-tail of the free inhibitor in an appropriate orientation for binding CPA (*33*). Thus, the increase in K_i observed for the Ala-substituted mutant can be attributed not only to loss of PCI−CPA contacts but also to an increase in flexibility (entropy) at the C-tail of this mutant. The 1D NMR spectrum of the F23A/W28A mutant, although it shows reduced signal dispersion compared to that of WT PCI, still corresponds to a protein with a compact three-dimensional structure. However, the low recombinant expression level of this mutant prevented the acquisition of 2D NMR spectra.

Oxidative Folding of PCI Forms. Oxidative refolding studies of PCI mutant forms were carried out in the absence (control −) and presence of redox agents. Folding intermediates were trapped by acidification at different times during the refolding process and analyzed by RP-HPLC. The assays were always performed in parallel with a control refolding experiment with WT PCI under the same conditions. The typical results observed for the refolding of WT PCI are shown in Figure 4 for selected times. The first stage of nonspecific packing of WT PCI to reach scrambled three-disulfide species is very quick, the consolidation of scrambled species being the major rate-limiting step. As previously reported, the disulfide reshuffling of the scrambled intermediates was very slow in the buffer without added thiols (control −), leading to a final trapped mixture with less than 10% of the native species at the end of the folding process. In contrast, in the presence of supplementing thiols (Cys or Cys and Cys-Cys), more than 90% of native PCI was

[3] F. X. Aviles et al., unpublished data.

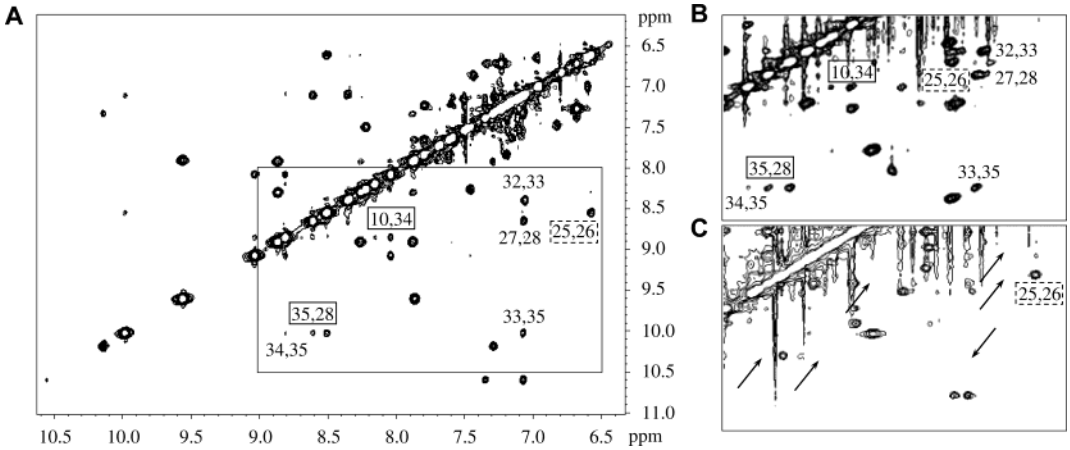

FIGURE 3: NH−NH regions of the NOESY spectra of WT (A), F23A (B), and W28A (C) PCI forms. NMR spectra were obtained at 35 °C and a protein concentration of 2 mM in 10% D_2O. Selected cross-peaks between amide protons are shown. The arrows denote WT cross-peaks absent in the mutant. The boxes denote long-range NOEs. The spectra are unsymmetrized.

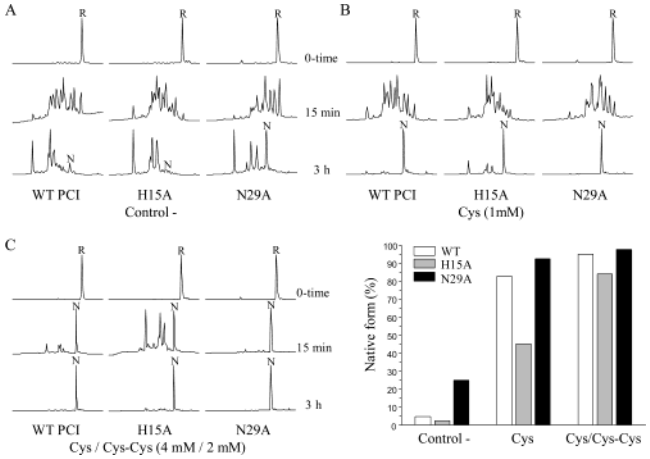

FIGURE 4: Oxidative folding of PCI forms in the presence of redox agents. The figure shows the oxidative refolding process of WT, H15A, and N29A PCI forms. Reduced and denatured PCIs were allowed to refold in Tris-HCl buffer (0.1 M, pH 8.4) in the absence (A, control −) and presence of (B) Cys (1 mM) or (C) Cys and Cys-Cys (4 and 2 mM, respectively). Acid-trapped intermediates were analyzed at the noted times by HPLC as described in detail in Experimental Procedures. N and R denote the elution positions of native and fully reduced species, respectively. The graphs show the percentages of native species for each PCI form obtained under different conditions (A−C) after 3 h of refolding, calculated from the peak areas in the corresponding HPLC chromatograms.

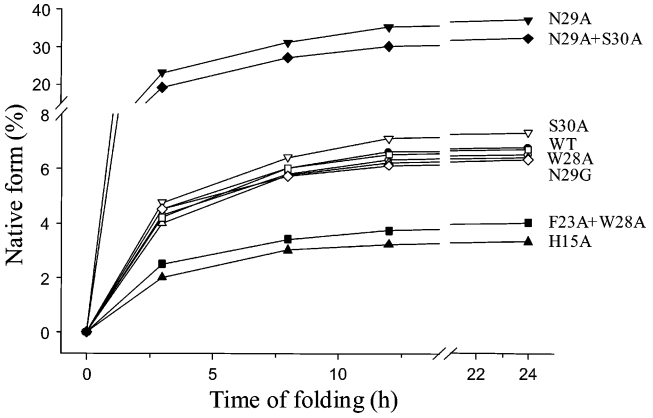

FIGURE 5: Folding kinetics of the different PCI forms. Refolding experiments with WT and PCI mutants were performed in the absence of redox agents (control −). Folding intermediates were trapped in a time course manner by acidification, and were then analyzed by HPLC. The symbols show the percentages of native species for the different PCI forms along the folding process, calculated from the peak areas in the corresponding HPLC chromatograms: WT (●), H15A (▲), W22A (○), F23A (△), W28A (□), F23A/W28A (■), N29A (▼), N29G (◇), S30A (▽), and N29A/S30A (◆).

recovered within 3 h of folding. In this reaction, Cys promotes the conversion of scrambled PCIs to the native form without accelerating the flow between fully reduced PCI and scrambled species or altering the apparent composition of one- and two-disulfide intermediates, whereas Cys-Cys drastically enhances the flow between reduced PCI and scrambled species (*20*).

The oxidative refolding of all Ala mutants was characterized in detail to test the role of the secondary binding site residues in the folding pathway of PCI. No differences were detected for any mutant, as compared with WT PCI, in the initial stage of nonspecific disulfide formation, either in folding speed or in intermediate heterogeneity. This is illustrated for some mutants in Figure 4. It has been argued that the second step (consolidation) in the refolding process of PCI is extremely slow, when compared to those of other small disulfide-rich proteins such as hirudin (*20*, *22*), because it requires the exposure of hydrophobic sites previously hidden in the scrambled species, increasing the enthalpic cost of the folding reaction (*20*). To test this hypothesis, we analyzed the folding process of W22A, F23A, and W28A PCI mutants. The folding speed and efficiency of these less hydrophobic variants were similar to that of the WT PCI (Figure 5). However, the double mutant F23A/W28A exhibited reduced folding efficiency with respect to the WT or singly mutated forms. This behavior does not seem to correspond to an additive effect in loss of hydrophobicity but, as the above-mentioned structural studies suggest, to a somehow altered native conformation.

With regard to the role of polar residues, no significant differences in the folding process were observed when Ser30 was substituted with Ala, while important changes were detected for the other polar residues in the secondary binding site (Figure 5). Thus, the H15A mutant exhibited slower folding kinetics than the WT form, together with lower percentages of the native form at the end of the folding reaction (∼50% of WT in control −). However, the most important changes in the folding process were those observed

in mutant N29A. Whereas its initial stage of folding was similar to that of WT PCI, as shown in Figure 4, the reshuffling process exhibited a high efficiency in the absence of added thiols, with percentages of the native form ~6-fold higher than those of WT PCI at the end of the process (see Figure 5). The reshuffling of scrambled species into the native form is considerably accelerated in this mutant: 2 times faster than in the WT form, both without supplementing thiols and with 2-mercaptoethanol, when the refolding is performed at a high protein concentration (0.5 mg/mL; see Experimental Procedures).

It is worth mentioning that Asn29 is located in a non-regular β-turn linking the two short antiparallel β-strands of PCI, between residues 26−28 and 33−35 (Figure 1). The analysis of the PCI−CPA crystal structure shows that the three residues in the turn following Asn29 (Ser30, Ala31, and Arg32) have ϕ and ψ angles that are out of the allowed regions in the Ramachandran plot. To test whether the N29A mutant is improving its folding efficiency just because a reduction of the side chain size will give rise to either less entropic cost, less strain, or more flexibility in this turn region, the folding process of a new mutant, in which Asn29 was substituted with Gly, was analyzed. Surprisingly, N29G folded with the same speed and efficiency as the wild-type (Figure 5), indicating that the efficient folding of the N29A variant can be attributed to the methyl group on the Ala29 side chain and very unlikely to an improved turn flexibility or reduced strain. The double mutant N29A/S30A exhibited the same accelerated kinetics and high folding efficiency as the N29A mutant. It clearly indicates a position-dependent effect of the Ala substitutions in this turn.

Conformational Stability of WT, N29A, N29G, and N29A/S30A PCI Forms. To study whether the improved folding efficiency of the N29A mutants can be related to a stabilization of the native state of the protein, we derived the denaturation curves of the WT and mutated forms. The extent of unfolding, and hence the equilibrium constant between scrambled species and the native proteins, was clearly dependent upon the strength of the denaturant (Figure 6A). On the basis of the concentration that is required to achieve the same extent of PCI denaturation, GdnHCl was ~5-fold more potent than urea, which was unable to fully denature any of the native forms, in agreement with previous reports (*28*, *34*, *35*). PCI, while being highly stable in front of GdnHCl, unfolds in a cooperative-like manner that suggests the progressive loss of noncovalent interactions during the unfolding event. The denaturation curves, calculated from the fraction percent of the PCI form converted to the scrambled isomers in the presence of the denaturant and thiol initiator, are shown in Figure 6A. The concentrations of GdnHCl required to achieve 50% denaturation were 2.4 and 1.9 M for N29A and N29A/S30A, respectively, and 1.2 M for the WT form, indicating that the relative stability of these mutants was significantly higher than that of the wild-type. The N29G mutant exhibited the same stability as WT PCI, in front of both urea and GdnHCl. The unfolding rate constants for WT and N29A PCI at 6, 7, and 8 M GdnHCl were found to be very similar (data not shown).

The conformational stability of WT and N29A PCI was also analyzed by deuterium to proton (D/H) exchange experiments followed by MALDI-TOF MS. The kinetics of interconversion were similar for both proteins, but the extent

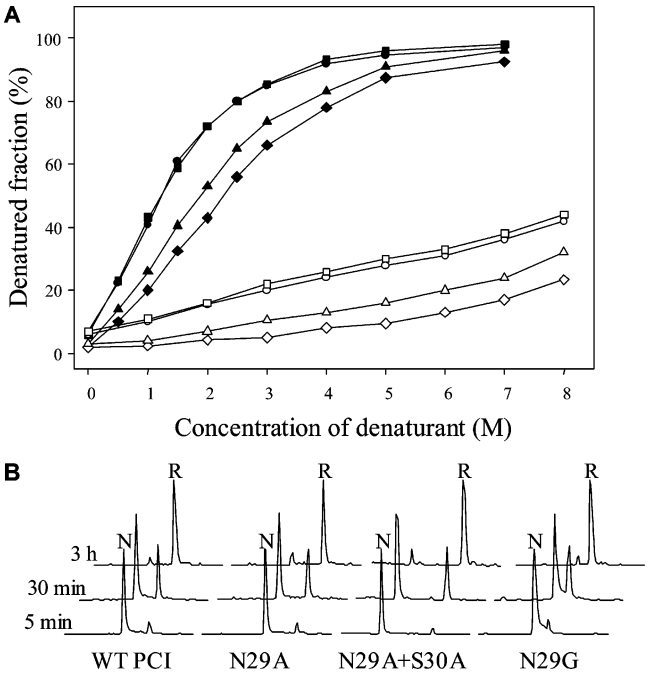

FIGURE 6: Denaturation curves and reductive unfolding of PCI forms. (A) The denatured fraction is the percentage of each PCI form that is converted to scrambled isomers. Data for WT, N29G, N29A, and N29A/S30A are depicted with the following symbols: ●, ■, ◆, and ▲, respectively. The denaturants used are GdnHCl (filled symbols) and urea (empty symbols). Denaturation was carried out at 23 °C, for 20 h, in Tris-HCl buffer (0.1 M, pH 8.4) containing 2-mercaptoethanol (0.25 mM) and the indicated concentration of denaturant. (B) Native WT PCI and N29A, N29A/S30A, and N29G mutants were treated with 5 mM dithiothreitol in Tris-HCl buffer (0.1 M, pH 8.4); the reactions were quenched with 2% aqueous trifluoroacetic acid, and the mixtures were analyzed by HPLC as described in Experimental Procedures. The peaks corresponding to native (N) and reduced (R) species are indicated.

of hydrogen exchange was fairly different. WT PCI only retains five deuterons at the end of the reaction because of its low secondary structure content, while the N29A mutant retains two additional protected deuterons. This 40% increase in the level of protected deuterons is in agreement with the increase in stability deduced from the denaturation curves. It is worth mentioning that the N29A mutant showed a recombinant expression yield approximately 2-fold higher than that of WT PCI, another indication of higher stability.

Structural Reasons behind the Improved Conformational Stability and Folding Efficiency of the N29A Form. The 228 nm spectral maximum related to the N-terminal Tyr37 environment in the CD spectrum of the N29A mutant is almost 2-fold more intense than in WT PCI (Figure 2). The minimum in ellipticity is located at 209 nm, instead of the 204 nm band typical for the WT form, and is also more intense. These features, and the sensitivity of such bands to denaturants (data not shown), suggest that this mutant is a more compact folded and structured protein.

The analyses of the 2D NOESY NMR spectra show an increase in the number and intensity of NOE contacts for the N29A form. Most of the new or stronger NOEs were observed in the NH−NH region involving residues Ala26−Gly35 (A26−G35, Q25−G35, C27−W28, W28−G35, A31−R32, R32−T33, C34−G35, and P36−T37) (Figure 7). Although Ala29 does not seem to be directly involved in

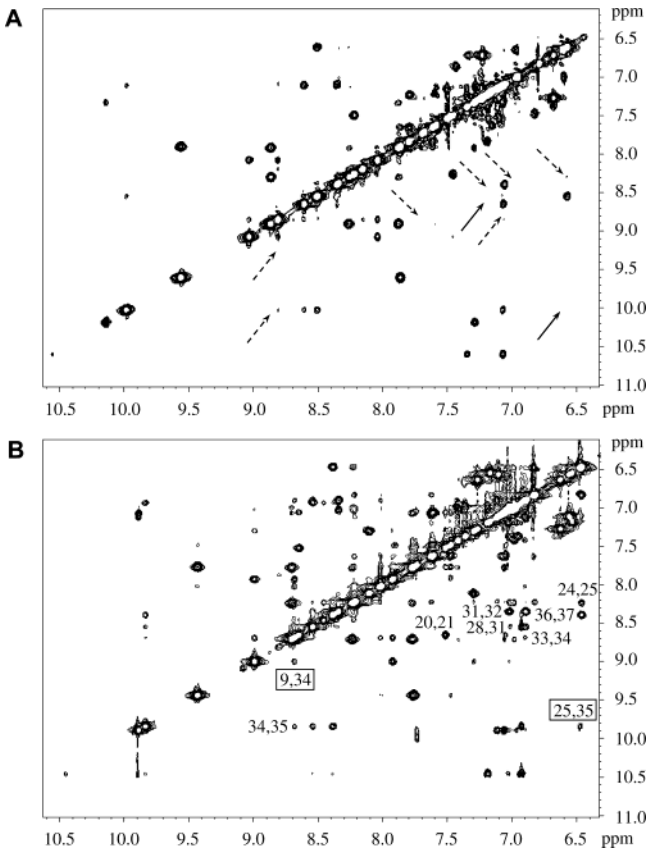

FIGURE 7: NH−NH regions of the NOESY spectra of WT (A) and N29A (B) PCI forms. The experimental conditions were the same as those described in the legend of Figure 3. Selected cross-peaks between amide protons are shown in the N29A spectrum. The cross-peaks absent in the WT form (vs the mutant) are denoted with arrows. The boxes denote long-range NOEs. The spectra are unsymmetrized.

any of the new contacts, they are indicative of stronger noncovalent interactions, and a more stable β-hairpin region.

Surprisingly, the change of Asn29 to Ala not only results in local changes but also has a long-range effect, since new contacts far away from the mutation point were observed, mainly located in the short 3_{10}-helix generated by two consecutive type III reverse turns between residues 14 and 19. The new NOEs are between C12−K13, C12−T33, K13−D17, D16−D17, and G20−A21. Interestingly enough, this 3_{10}-helix constitutes, together with the above-mentioned short β-sheet, the only secondary structure elements in PCI.

Mechanism of Reductive Unfolding of WT, N29A, N29G, and N29A/S30A PCI Forms. In the absence of denaturant, a high concentration of the reducing agent is needed to break the three PCI native disulfides (*28*). Reduction of the three native disulfide bonds of this protein follows the "all-or-none" mechanism observed in numerous small single-domain proteins such as hirudin and TAP (*18*, *36*). In this mechanism, reduction of the first disulfide bond is a rate-limiting step, after which the remaining cystines are quickly reduced, there is little accumulation of partially reduced species, and protein structure is lost.

Reduction of WT, N29A, N29G, and N29A/S30A PCI at a fixed concentration of dithiothreitol (5 mM) was followed over time to test whether the additional noncovalent forces present in the N29A variant may influence the reductive unfolding reaction of PCI. Under this condition, reduction of the three native disulfide bonds of these proteins followed the described all-or-none mechanism (Figure 6B), suggesting that their native disulfide bonds are stabilized in a concerted and interdependent manner (*18*). Kinetic analysis revealed that the reduction rates of these proteins were identical (data not shown).

Relationship between Conformational Stability and Structural Uniqueness in PCI. Our group previously reported that when native PCI is incubated in a physiological buffer (pH 7.4−8.4) containing trace amounts of a thiol agent, a minute fraction of the protein spontaneously shuffles its native disulfide bonds and isomerizes to form scrambled species (*28*). To study whether there is any relationship between conformational stability and the ratio of non-native ensembles under physiological conditions, the equilibrium constant for some PCI variants with altered stability was determined in the presence of 0.25 mM 2-mercaptoethanol to "jump start" such spontaneous conversion. The reaction reached a state of equilibrium after 24 h, and the percentages of scrambled species for the different variants were as follows: 6% for WT ($K'_{eq} = 0.06$, $\Delta G_d^\circ = 1.7$ kcal/mol), 7% for N29G ($K'_{eq} = 0.07$, $\Delta G_d^\circ = 1.6$ kcal/mol), 2% for N29A ($K'_{eq} = 0.02$, $\Delta G_d^\circ = 2.3$ kcal/mol), 3% for N29A/S30A ($K'_{eq} = 0.03$, $\Delta G_d^\circ = 2.1$ kcal/mol), and 14% for W28A ($K'_{eq} = 0.14$, $\Delta G_d^\circ = 1.2$ kcal/mol).

DISCUSSION

Role of the PCI Secondary Binding Site in CPA Inhibition. Although the structure of the PCI−CPA complex is relatively well-known, the knowledge of the basis of the complex formation and of its thermodynamic stability is still scarce. To gain insight into the latter issues, our group previously analyzed the contribution of C-tail residues of PCI to the binding to CPA (*14*, *15*). Such analysis dissected the role played by each residue in the PCI primary binding site and suggested a significant involvement of the secondary binding site residues in the interaction. Our study shows that the polar residues in the secondary binding region of PCI (His15, Asn29, and Ser30) are not likely to be involved in the stabilization of the PCI−CPA complex, whereas aromatic residues (Trp22, Phe23, and Trp28) appear to play an important role in it since ~30% of the free energy of binding can be attributed to them.

A common feature of proteins with the cysteine knot fold is the presence of large hydrophobic patches on the protein surface, which are stabilized by the covalent disulfide scaffold when function requires those large hydrophobic surfaces to be exposed in small volumes (*13*). This is also the case for PCI, where the surface aromatic patch formed by residues 22, 23, and 28 is an important factor in its inhibitory activity. Our studies allow us to dissect the individual contribution of each side chain in this patch. The structural results in this work show that the F23A mutant keeps a structure very similar to that of WT PCI, whereas W28A loses some of the contacts between the secondary contact region and the C-tail present in the WT form. Therefore, although both residues are basic for PCI function, as deduced from the weak inhibitory capability of their Ala mutants, they clearly play different roles in this interaction. The importance of Phe23 in the binding of PCI to CPA can probably be attributed to the interactions established between

its aromatic side chain and the carboxypeptidase surface. In contrast, the importance of Trp28 seems to depend on the maintenance of the C-terminal tail in a proper orientation, providing the conformational rigidity needed for the binding to the enzyme. These observations may facilitate the rational improvement of the PCI inhibitory properties toward carboxypeptidases.

Structural Reasons behind the Low Folding Efficiency of PCI. The folding mechanism of several small disulfide-rich proteins, such as PCI, hirudin, and TAP, can be clearly dissected in two distinct stages (*20*, *22*, *26*). An initial stage of nonspecific disulfide pairing leads to the formation of scrambled species as the crucial folding intermediates. The final stage of the folding process involves the reshuffling of the scrambled disulfides into the native conformation. For these proteins, the folding forces from noncovalent bonds alone are apparently insufficient to drive the unfolded protein across the energy barrier, and a reduction of the conformational search by disulfide bond formations is needed. It is only at the final stage of folding where the attainment of the native structure is probably driven by noncovalent interactions (*18*, *20*). According to this theory, the second stage of folding in PCI, which contains fewer noncovalent bonds than hirudin or TAP, is extremely inefficient compared to these topologically related proteins.

Two alternative explanations have been proposed for the very slow consolidation process of PCI (*20*). First, its disulfide structure is different from that in hirudin and TAP, also with three disulfide bonds: the two disulfides linking sequences, Cys8-Asn-Lys-Pro-Cys12 and Cys24-Glu-Ala-Cys27, form a ring to which the third disulfide (Cys18−Cys34) is threaded. This tight conformation has been suggested to impose structural constraints and prevent efficient formation of the native structure. However, our finding that some PCI mutants that display the same disulfide pattern exhibit striking improved folding efficiencies runs against this hypothesis. Second, in PCI, unlike in hirudin and TAP, the scrambled forms are less hydrophobic than the properly folded protein, suggesting that an exposition of previously hidden hydrophobic sites occurs during the consolidation process with the consequent enthalpic cost. From our studies, however, it is clear that the unfavorable change in environment suffered by the hydrophobic side chains of PCI during the consolidation process does not increase the energy barrier of the folding reaction, since the truncation of side chains of W22, F23, or W28 with an Ala mutation does not change either the folding speed or the efficiency, ruling out this hypothesis.

In this work, we have found that the N29A variant exhibits a high refolding efficiency and an accelerated reshuffling process in comparison to WT PCI. In the PCI−CPA crystal structure, Asn29 is located in a nonregular reverse turn that lacks the characteristic 4−1 hydrogen bond and links the two short antiparallel β-strands of PCI (*12*). In this crystal structure, the ϕ and ψ dihedral angles for the second and third residues of this turn are located in disallowed areas of the Ramachandran plot. Steric clashes make protein folding energetically expensive in this zone and may constitute yet another reason for PCI low folding efficiency. The reduction in side chain size in the N29A mutant may relax the strain in this area by promoting a more canonical conformation or an increased flexibility. Mutant N29G, expected to perform equal or better than N29A, folded in a manner similar to that of the WT form, showing that the improved characteristics of N29A variants are not related to better turn properties but rather restricted to the effect of the Ala29 side chain. These results agree with the refined structure of free PCI in solution reported by our group "during the development of the present work" (*11*). In the NMR structure, this turn is more regular and relaxed than that in the complex of PCI with CPA, indicating a clear conformational shift of this turn upon enzyme binding. In solution, this type III β-turn exhibits the characteristic CO(i)−NH(i + 3) backbone hydrogen bonds, and in addition, all turn residues of free PCI are distributed in favorable regions of the Ramachandran plot.

Thus, according to our results, the higher folding efficiency of the N29A mutant can be attributed unequivocally to the effect of the methyl group of the Ala side chain. CD and NMR studies show that N29A is more compact and structured than the WT, probably as a result of both new short- and long-range effects. Locally, the short β-sheet including this turn appears to be stabilized by the presence of more contacts between the two β-strands. Interestingly, some of the new long-range noncovalent contacts are observed between this region and the 3_{10}-helix of PCI, thus connecting the only structured regions of this small molecule. In PCI, it is the difficult consolidation of the scrambled isomers into the native form that makes its folding process extremely inefficient as compared to those of other similar proteins. In the case of N29A, the mutation introduces new noncovalent interactions that drive more efficiently this stage of reshuffling, leading to a higher efficiency of the folding reaction. All these points indicate that the low efficiency of folding exhibited by PCI is probably due to the scarce noncovalent contacts displayed by this molecule.

Conformational Stability and Structural Uniqueness in PCI. PCI is a very stable fold probably designed to resist hard external conditions and still be functional (*35*). The conformational stability of N29A mutants is significantly higher than that of WT PCI, as deduced from their denaturation curves, and correlates with a higher refolding efficiency. The introduction of new long- and short-range interactions in N29A decreases the free energy of the native state of PCI and renders it less susceptible to denaturation. The deuterium to proton exchange method monitored by MS (*37*), also applied to characterize the conformational stability of this mutant relative to the WT form, shows an increase in the amount of deuterons retained by the N29A mutant. It agrees with the data from its denaturation curves and NMR spectra, establishing a relationship between protection to D/H exchange and stability and/or compactness. While both new short- and long-range interactions would contribute to the increased protein stability, long-range contacts would lead to increased compactness.

PCI is unable to fold quantitatively into a single structure under physiological conditions, following a behavior of "one-sequence multiple structures" involving the formation of native and scrambled species (*28*). Our data show that these non-native low-energy packing alternatives (scrambled species) indeed exist in PCI in a state of equilibrium with the native structure. We observed that N29A-containing variants occur with smaller amounts of scrambled species in equilibrium than with WT PCI, whereas in less stable variants, such as W28A, the equilibrium is more displaced toward

the non-native conformations, thus confirming that there is a correlation between the conformational stability of the native ensemble and its structural uniqueness. For a polypeptide chain to fold into a unique conformation, a free energy gap of several kilocalories per mole between the correctly folded protein and alternative folds is required. As we show, increasing this gap by lowering the free energy of the native ensemble will also increase its structural uniqueness. Our observations are in total agreement with those made in proteins causing conformational diseases where stabilization of the native structure has been used as a tool to restrict conformational fluctuations that may drive aggregation of prone ensembles (*38*).

Biological and Biotechnological Implications. It is interesting to note that the primary site of binding of PCI to CPA is located in a region, the C-tail, that is much less important for its conformation and folding than the secondary binding site. Although both sites are conformationally and functionally inter-related, as we have shown in this work, it is surprising that the secondary binding site resides in a region so critical for the folding of this protein, a potential constraint for functional evolution. The comparison of PCI with other proteic inhibitors of metallocarboxypeptidases shows that the C-tail structure is much more conserved than that of the secondary binding site (*5*). The latter is located in a region of the protein that changes in both composition and topology from one inhibitor to another. Such structural characteristics are probably important factors in the evolution of these proteins, which would be the consequence of the convergent evolution dictated by the target molecules, the carboxypeptidases (*39*). The features of the primary and secondary binding sites of PCI described above should be taken into account when used as a lead compound for drug design. Actually, PCI has been proposed as a potential fibrinolytic agent for treatment and/or prevention of thrombotic diseases (*40*−*42*) because of its ability to inhibit plasma CPB (TAFI) (*43*), and great interest in the design of minimized inhibitors appeared (*44*).

ACKNOWLEDGMENT

We are grateful to Drs. S. Bronsoms, G. Venhudova, and F. Canals for technical assistance and helpful discussions. We also thank O. Conchillo for computational support.

REFERENCES

1. Otlewski, J., and Apostoluk, W. (1997) Structural and energetic aspects of protein−protein recognition, *Acta Biochim. Pol. 44*, 367−387.
2. Edwards, A. M., Kus, B., Jansen, R., Greenbaum, D., Greenbatt, J., and Gerstein, M. (2002) Bridging structural biology and genomics: assessing protein interaction data with known complexes, *Trends Genet. 18*, 529−536.
3. Nooren, I. M., and Thornton, J. M. (2003) Diversity of protein−protein interactions, *EMBO J. 22*, 3486−3492.
4. Bode, W., and Huber, R. (2000) Structural basis of the endoproteinase-protein inhibitor interaction, *Biochim. Biophys. Acta 1477*, 241−252.
5. Vendrell, J., Querol, E., and Aviles, F. X. (2000) Metallocarboxypeptidases and their protein inhibitors. Structure, function and biomedical properties, *Biochim. Biophys. Acta 1477*, 284−298.
6. Coughlin, S. R. (2000) Thrombin signalling and protease-activated receptors, *Nature 14*, 258−264.
7. Turk, B., Stoka, V., Rozman-Pungercar, J., Cirman, T., Droga-Mazovec, G., Oreic, K., and Turk, V. (2002) Apoptotic pathways: involvement of lysosomal proteases, *Biol. Chem. 383*, 1035−1044.
8. Stamenkovic, I. (2003) Extracellular matrix remodelling: the role of matrix metalloproteinases, *J. Pathol. 200*, 448−464.
9. Hass, G. M., and Ryan, C. A. (1981) Carboxypeptidase inhibitor from potatoes, *Methods Enzymol. 80*, 778−791.
10. Clore, G. M., Gronenborn, A. M., Nilges, M., and Ryan, C. A. (1987) Three-dimensional structure of potato carboxypeptidase inhibitor in solution. A study using nuclear magnetic resonance, distance geometry, and restrained molecular dynamics, *Biochemistry 26*, 8012−8023.
11. Gonzalez, C., Neira, J. L., Ventura, S., Bronsoms, S., Rico, M., and Aviles, F. X. (2003) Structure and dynamics of the potato carboxypeptidase inhibitor by ^{1}H and ^{15}N NMR, *Proteins 50*, 410−422.
12. Rees, D. C., and Lipscomb, W. N. (1982) Refined crystal structure of the potato inhibitor complex of carboxypeptidase A at 2.5 Å resolution, *J. Mol. Biol. 160*, 475−498.
13. Lin, S. L., and Nussinov, R. (1995) A disulphide-reinforced structural scaffold shared by small proteins with diverse functions, *Nat. Struct. Biol. 2*, 835−837.
14. Molina, M. A., Marino, C., Oliva, B., Aviles, F. X., and Querol, E. (1994) C-tail valine is a key residue for stabilization of complex between potato inhibitor and carboxypeptidase A, *J. Biol. Chem. 269*, 21467−21472.
15. Marino-Buslje, C., Venhudova, G., Molina, M. A., Oliva, B., Jorba, X., Canals, F., Aviles, F. X., and Querol, E. (2000) Contribution of C-tail residues of potato carboxypeptidase inhibitor to the binding to carboxypeptidase A. A mutagenesis analysis, *Eur. J. Biochem. 267*, 1502−1509.
16. Creighton, T. E. (1986) Disulfide bonds as probes of protein folding pathways, *Methods Enzymol. 131*, 83−106.
17. Creighton, T. E. (1990) Protein folding, *Biochem. J. 270*, 1−16.
18. Chang, J. Y. (1997) A two-stage mechanism for the reductive unfolding of disulfide-containing proteins, *J. Biol. Chem. 272*, 69−75.
19. Chang, J. Y. (1999) Denatured states of tick anticoagulant peptide. Compositional analysis of unfolded scrambled isomers, *J. Biol. Chem. 274*, 123−128.
20. Chang, J. Y., Canals, F., Schindler, P., Querol, E., and Aviles, F. X. (1994) The disulfide folding pathway of potato carboxypeptidase inhibitor, *J. Biol. Chem. 269*, 22087−22094.
21. Venhudova, G., Canals, F., Querol, E., and Aviles, F. X. (2001) Mutations in the N- and C-terminal tails of potato carboxypeptidase inhibitor influence its oxidative refolding process at the reshuffling stage, *J. Biol. Chem. 276*, 11683−11690.
22. Chatrenet, B., and Chang, J. Y. (1993) The disulfide folding pathway of hirudin elucidated by stop/go folding experiments, *J. Biol. Chem. 268*, 20988−20996.
23. Chang, J. Y. (1994) Controlling the speed of hirudin folding, *Biochem. J. 300*, 643−650.
24. Wu, J., Yang, Y., and Watson, J. T. (1998) Trapping of intermediates during the refolding of recombinant human epidermal growth factor (hEGF) by cyanylation, and subsequent structural elucidation by mass spectrometry, *Protein Sci. 7*, 1017−1028.
25. Chang, J. Y., Li, L., and Lai, P. H. (2001) A major kinetic trap for the oxidative folding of human epidermal growth factor, *J. Biol. Chem. 276*, 4845−4852.
26. Chang, J. Y. (1996) The disulfide folding pathway of tick anticoagulant peptide (TAP), a Kunitz-type inhibitor structurally homologous to BPTI, *Biochemistry 35*, 11702−11709.
27. Chang, J. Y., and Ballatore, A. (2000) Structure and heterogeneity of the one- and two-disulfide folding intermediates of tick anticoagulant peptide, *J. Protein Chem. 19*, 299−310.
28. Chang, J. Y., Li, L., Canals, F., and Aviles, F. X. (2000) The unfolding pathway and conformational stability of potato carboxypeptidase inhibitor, *J. Biol. Chem. 275*, 14205−14211.
29. Cunningham, B. C., and Wells, J. A. (1989) High-resolution epitope mapping of hGH-receptor interactions by alanine-scanning mutagenesis, *Science 244*, 1081−1085.
30. Ashkenazi, A., Presta, L. G., Marsters, S. A., Camerato, T. R., Rosenthal, K. A., Fendly, B. M., and Capon, D. J. (1990) Mapping the CD4 binding site for human immunodeficiency virus by alanine-scanning mutagenesis, *Proc. Natl. Acad. Sci. U.S.A. 87*, 7150−7154.
31. Molina, M. A., Avilés, F. X., and Querol, E. (1992) Expression of a synthetic gene encoding potato carboxypeptidase inhibitor using a bacterial secretion vector, *Gene 116*, 129−138.

32. Morrison, J. F. (1982) The slow-binding and slow, tight-binding inhibition of enzyne-catalysed reactions, *Trends Biochem. Sci. 7*, 102−105.
33. Oliva, B., Wästlund, M., Nilsson, O., Cardenas, R., Querol, E., Avilés, F. X., and Tapia, O. (1991) Stability and fluctuations of the potato carboxypeptidase A protein inhibitor fold: a molecular dynamics study, *Biochem. Biophys. Res. Commun. 176*, 616−621.
34. Bulychev, A., and Chang, J. Y. (1999) Unfolding of hirudin characterized by the composition of denatured scrambled isomers, *J. Protein Chem. 18*, 771−778.
35. Salamanca, S., Villegas, V., Vendrell, J., Li, L., Aviles, F. X., and Chang, J. Y. (2002) The unfolding pathway of leech carboxypeptidase inhibitor, *J. Biol. Chem. 277*, 17538−17543.
36. Chang, J. Y., Li, L., and Bulychev, A. (2000) The underlying mechanism for the diversity of disulfide folding pathways, *J. Biol. Chem. 275*, 8287−8289.
37. Villanueva, J., Canals, F., Villegas, V., Querol, E., and Aviles, F. X. (2000) Hydrogen exchange monitored by MALDI-TOF mass spectrometry for rapid characterization of the stability and conformation of proteins, *FEBS Lett. 472*, 27−33.
38. Chiti, F., Taddei, N., Bucciantini, M., White, P., Ramponi, G., and Dobson, C. M. (2000) Mutational analysis of the propensity for amyloid formation by a globular protein, *EMBO J. 19*, 1441−1449.
39. Reverter, D., Vendrell, J., Canals, F., Horstmann, J., Aviles, F. X., Fritz, H., and Sommerhoff, C. P. (1998) A carboxypeptidase inhibitor from the medical leech *Hirudo medicinalis*. Isolation, sequence analysis, cDNA cloning, recombinant expression, and characterization, *J. Biol. Chem. 273*, 32927−32933.
40. Nagashima, M., Werner, M., Wang, M., Zhao, L., Light, D. R., Pagila, R., Morser, J., and Verhallen, P. (2000) An inhibitor of activated thrombin-activatable fibrinolysis inhibitor potentiates tissue-type plasminogen activator-induced thrombolysis in a rabbit jugular vein thrombolysis model, *Thromb. Res. 98*, 333−342.
41. Schneider, M., and Nesheim, M. (2003) Reversible inhibitors of TAFIa can both promote and inhibit fibrinolysis, *J. Thromb. Haemostasis 1*, 147−154.
42. Walker, J. B., Hughes, B., James, I., Haddock, P., Kluft, C., and Bajzar, L. (2003) Stabilization versus inhibition of TAFIa by competitive inhibitors in vitro, *J. Biol. Chem. 278*, 8913−8921.
43. Bouma, B. N., and Meijers, J. C. M. (2003) Thrombin-activatable fibrinolysis inhibitor (TAFI, plasma procarboxypeptidase B, procarboxypeptidase R, procarboxypeptidase U), *J. Thromb. Haemostasis 1*, 1566−1574.
44. Barrow, J. C., Nantermet, P. G., Stauffer, S. R., Ngo, P. L., Steinbeiser, M. A., Mao, S. S., Carroll, S. S., Bailey, C., Colussi, D., Bosserman, M., Burlein, C., Cook, J. J., Sitko, G., Tiller, P. R., Miller-Stein, C. M., Rose, M., McMasters, D. R., Vacca, J. P., and Selnick, H. G. (2003) Synthesis and evaluation of imidazole acetic acid inhibitors of activated thrombin-activatable fibrinolysis inhibitor as novel antithrombotics, *J. Med. Chem. 46*, 5294−5297.

BI049596J